Eidgenössische Technische Hochschule Zürich
Swiss Federal Institute of Technology Zurich

Neural Control of Movement

Dynamic Causal Modelling During Intuitive Physical Inference

Semester Project

Yihui Du
yihudu@student.ethz.ch

Neural Control of Movement Laboratory
Department of Health Sciences and Technology, D-HEST
ETH Zürich

Supervisors:
Gabrielle Zbären
Prof. Dr. Nicole Wenderoth

21.03.2022 – 30.06.2022

Abstract

Most common objects in the real world conform to Newtonian principles of motion. Our brain is capable of making quick intuitive estimations of physical quantities in the physical world such as mass, velocity, momentum. To investigate the functional neural mechanism underlying physical inference, we designed event-related fMRI experiments and applied several computational models to analyse data. Each subject in the experiment was required to complete two parallel tasks, in which the subject imagined and estimated the object's falling time during the simulation task, while during the perception task the subject received direct visual stimuli of the falling object. The conjunction of the general linear model (GLM) analysis results revealed several overlapping activated brain regions during physical inference and perception tasks. The dynamic causal modelling (DCM) was then applied to analyze the extracted timeseries of blood oxygen-level dependent (BOLD) signals from three brain regions to reveal the dynamics of neural connections during physical inference. The DCM results of visual perception task revealed decreased self-inhibition on early visual cortex. Furthermore, the DCM results validated the presence of driving inputs in higher functional brain areas and top-down modulation of connectivity during physical inference task.

Contents

1. Introduction

How do the humans have a quick intuitive grasp of the world's physical structure and dynamics is an interesting question about physical inference. For instance, we see that the pool supports the laptop unsteadily (figure 1, upper right) and we can easily know intuitively that the laptop would fall in the water or on the ground if the pool were pressed. Such physical scene understandings link perception with higher cognition, but the neural mechanisms underlying them in the brain remain unclear.

Early studies of intuitive physics inference suggested that there might be a mental "intuitive physics Engine" (IPE) model in the brain, a cognitive mechanism like computer engines that simulate rich physics in video games (1). Subsequent work has found that early visual cortex regions encode visual imagery and might be involved in physical inference (2). Several recent fMRI experiments identified a set of brain regions that implements fast intuitive physical inference from visually presented scenes (3). However, all these works address only independent brain regions or computational framework associated with intuitive physical inference. Our goal here is to build an effective connectivity network of the overlapping activated brain regions in inference task and perception task, based on the neural dynamic causal modelling (DCM) of the extracted timeseries of BOLD signals, to reveal the neural mechanisms under physical inference.

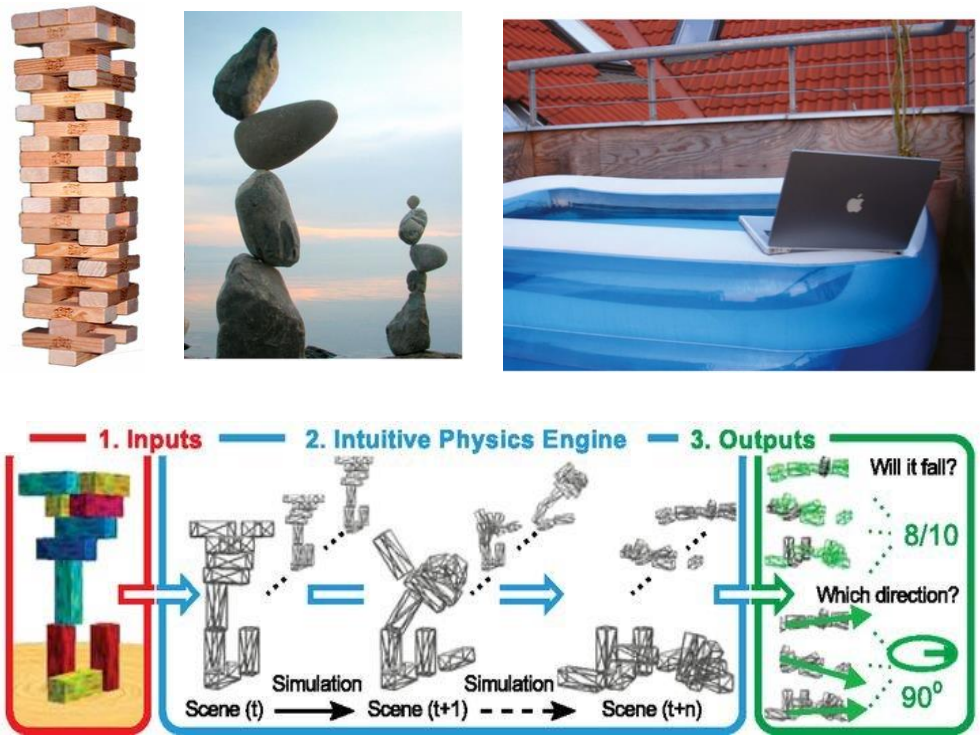

Figure 1: The upper row shows some daily life scenarios that involve physical inference such as stability inference (1, 3). The bottom row shows the proposed intuitive physics engine (IPE) model (1).

In the event-related fMRI tasks, the experimental stimulation causes changes in neural activity, and the neural activity in turn causes the BOLD response, which we observe via the scanner. We are interested in the hidden neural activity, which we cannot directly observe, so it must be inferred with DCM. The application of DCM is to assess effective connectivity – the directed causal influences among brain regions – or more simply the effect of one region on another. Based on the conjunction analysis of the general linear model (GLM) results of our designed simulation and perception tasks, in total three brain areas – superior parietal lobule (SPL), supramarginal gyrus (SMG), and early visual cortex (V1/V2) – are selected as regions of interest (ROIs) for DCM. We hypothesize distinct context sensitive patterns of top-down and bottom-up influences during physical inference compared to perception. The DCM are applied to test whether the driving inputs exist in visual cortex regions or parietal regions (SMG and SPL), and whether the modulatory inputs are bottom-up or top-down modulations during physical inference task.

2. Materials and Methods

2.1. Subjects

To conduct our designed fMRI experiments, in total 20 healthy adult participants (12 females, 8 males, age range 21–52) were recruited. Four (2 females, 2 males) of those 20 participants were excluded from the subsequent analyses because of their incorrect task execution.

2.2. Experimental task

Each participant was required to complete a total of 6 runs in the physical inference task, and 1 run in the perception task, resulting in a total scanning time of approximately 70 minutes per participant. Each run of the physical inference task consists of 6 sessions, including crossover appearances of 3 simulation sessions and 3 control sessions, and each session contains 6 repeated trials. The interscan interval (the repetition time, TR) is 2.5 seconds per scan.

One trial of the physical inference task, which is referred to as “BALL Simulation” condition, works as follows (figure 2, left top row): An orange box with a ball attached to it enters the screen from either side and moves horizontally with a certain height and velocity. When the box drops the ball, an occluder appears simultaneously for participants to press the button as soon as they imagine the ball to land. Only one “catch trial” every six trials in the simulation session, the participants need to move the black bar to their estimated landing location of the ball. During the entire task there is a fixation cross in the middle of the screen, which the participants were asked to focus their vision on. This ensured that there were no unnecessary eye movements and increased standardization among different participants.

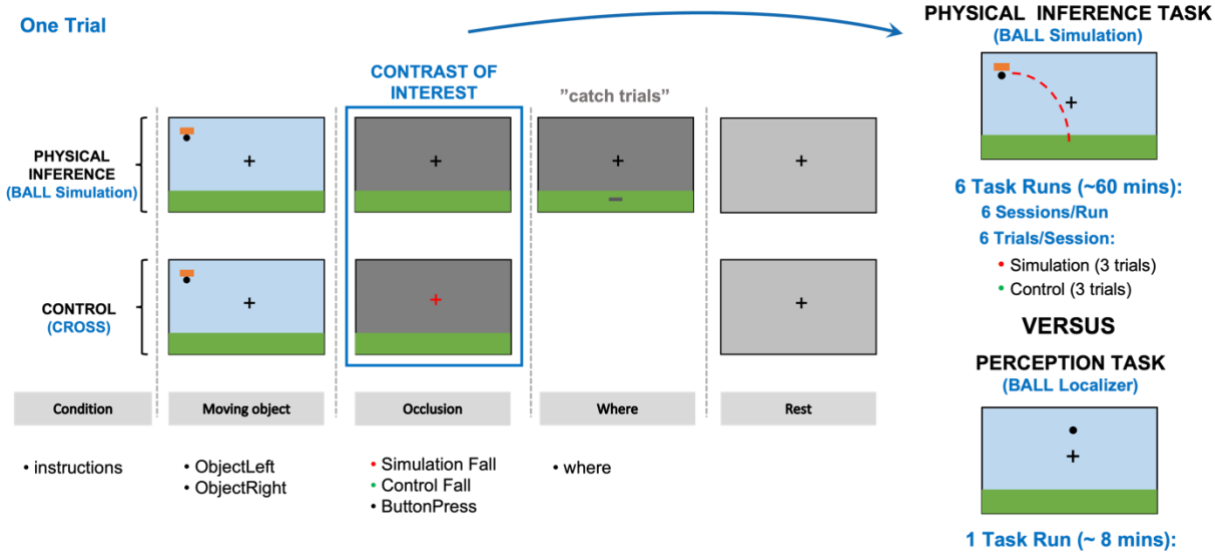

Figure 2: Intuitive physical inference fMRI experiment paradigm. The left panel shows one sample sequence of the simulation and control trials that the subjects need to react with in the fMRI scanner. The occlusion-column are the time frames used for the contrast of interest in the GLM analysis. The top right panel shows the occluded scene of the falling ball that the subjects need to imagine. The bottom right panel shows the scene of the falling ball that was seen by the subjects in the perception task.

The control trial of the physical inference task, which is called “CROSS” condition (figure 2, left bottom row), is similar as the BALL Simulation trial, except that the participant need to press the button as soon as the color of the fixation cross changed, instead of having to imagine the landing time of the ball. During this control trial, the participants received the same visual inputs and performed the same hand movements as in the BALL Simulation trial, but without imagining and predicting the time and location of the falling time.

During the parallel perception task, which is referred to as “Localizer” task (figure 2, right bottom panel), participants only need to directly watch the ball falling multiple times without having to imagine the falling time and location of the ball behind the occlude or having to press the button.

2.3. fMRI univariate analysis

To identify the ROIs related with simulation and perception tasks, we performed univariate contrast analysis on the acquired and pre-processed fMRI data. All analyses were performed using the statistical parametric mapping (SPM12) software and customized MATLAB scripts.

The general linear model (GLM) analysis was first specified and estimated on the single-subject level, with data and regressors concatenated over runs for the subsequent timeseries extraction. For the simulation task, the regressors of interest (figure 2, left) consist of onsets and durations of 7 combined task conditions (instructions, object appearance, simulation trial, control trial, catch trial, button press, no button press). The nuisance regressors include white matter (WM) timeseries, cerebrospinal fluid (CSF) timeseries, and six movement parameters, together with scrubbing regressors that scrub off any volume displaying motion bigger than half a voxel size. In general, the design matrix for the first-level GLM consists 14 regressors of interest including 7 conditions together with their temporal derivations, and 8 nuisance regressors with scrubbing timepoints.

We performed t-test ($p<0.001$ uncorrected) contrasts between the simulation condition and control condition to inference the voxels that showed significant higher activities during simulation trials than control trials (simulation > control). Additionally, an F-test contrast was calculated to identify all ‘Effects of interest’ – to later regress out any uninteresting effects such as head motion or breathing from the timeseries. This F-contrast was an identity matrix of dimension n ($n = 14$), where the first n columns in the design matrix related to interesting experimental effects.

For the perception task, the design matrix contains onsets and durations for ball falling as regressors of interest, combined with similar nuisance regressors as in the simulation task. The t-test ($p<0.001$ uncorrected) contrasts between ball falling condition and baseline are performed to inference the voxels that show significant positive activities during localizer task (local-fall > 0). A similar F-test of ‘Effects of interest’ was calculated as for the simulation task, with $n = 2$.

In the subsequent group-level GLM analysis, the contrast images from first-level results for every subject are collected for the one-sample summarized t-test ($p<0.001$ uncorrected) to find the brain regions that have significant contrasted activities among all 16 subjects. The group-level GLM functional images are mapped to the anatomy atlas to help the following definition of the

coordinates of ROIs (4). The conjunction analysis – an overlay of the contrast map of the second-level GLM results of both tasks – are then performed to help decide three brain areas as our ROIs for the following DCM analysis.

2.4. Dynamic causal modelling (DCM)

2.4.1. Timeseries extraction of regions of interest

We selected three regions of interest (ROIs) for our connectivity model based on the conjunction analysis of the GLM analysing results of the simulation and perception tasks (figure 3). To allow for the subject-specificity for the exact selection of the location of effect, we selected the ROI for each participant as an 8 mm sphere, whose centre is the local maximum of the contrast image ($p<0.05$ uncorrected) within the 16 mm sphere centred on the group peak in space. This approach ensures that the subject-specific ROIs are close to the average group activity, while allowing for slight variation in functional anatomy between participants.

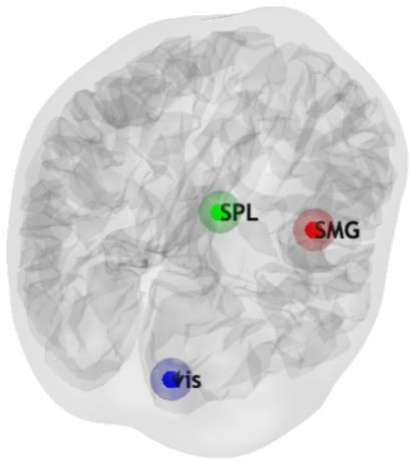

Region name	Location (mm)
Early Visual Cortex (**V1/V2**)	9 -88 -14
Superior Parietal Lobule (**SPL**)	12 -66 56
Supramarginal Gyrus (**SMG**)	40 -42 42

Figure 3: Group peak locations and coordinates of the three selected ROIs for DCM signal timeseries extraction.

For each subject, timeseries were extracted from every voxel in each of the contrast-masked ROIs. The signals were subsequently adjusted based on the F-contrast that retained the experimental effects of interest and regressed out task-unrelated variance specified by nuisance regressors. The first principal component (eigenvariate) of each region's adjusted data was then calculated as the timeseries for subsequent DCM analysis.

2.4.2. DCM specification

To quantify the effects of physical inference and perception on effective connectivity between the ROIs, we applied dynamic causal modelling (DCM) (5). The classical deterministic DCM uses the following bilinear state temporal differential equation to infer effective connectivity parameters, which is a Taylor approximation of the neuronal dynamic function:

$$\dot{z} = \left(A + \sum_{j=1}^{M} u_j B^j\right) z + Cu$$

The variable *z* describes neuronal activity resulting from the dynamic interplay of three different influences. First, the *A* matrix represents endogenous or fixed connectivity during baseline condition, without external stimulation. Second, the elements in *B* matrix represent the changes in connectivity modulated by experimental influences *u*. Finally, the matrix *C* denotes the direct influence of each experimental input *u*. We selected the condition ('simFall' and 'locFall') separately from the design matrix as the experimental input *u*. This neuronal model is coupled to a hemodynamic model of neurovascular coupling and the BOLD response, which together predict the BOLD timeseries (6). After DCM specification, the model is inverted to estimate the neural connective parameters by maximising the defined negative free energy. The slice timing model within DCM was set to the default value of 0.5 TR. The echo time (TE) of the scanner in both tasks was 35 ms.

Importantly, each brain region in this model is equipped with an inhibitory self-connection, specified by the elements on the leading diagonal of the average connectivity matrix *A* and modulatory input matrices *B* (7). This is implemented by splitting the connectivity matrix *A* and modulatory matrices *B* into two parts: extrinsic between-region connectivity and intrinsic within-region self-inhibition, with -0.5*Hz* as the default strength of the self-connections. Therefore, the more positive the self-connection parameter, the more self-inhibited the region, and so the less it will respond to inputs from the network. Conversely, the more negative the self-connection parameter, the less inhibited the region. For the extrinsic connectivity between regions, if it is positive the connection is excitatory, and if it is negative then the connection is inhibitory.

2.4.3. Connectivity parameter estimation and comparison

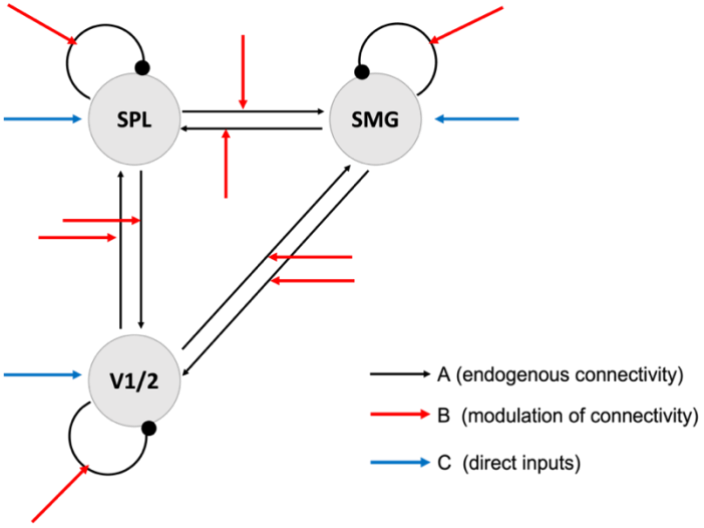

Figure 4: The network structure of our defined bilinear two-state DCM full model.

For the group-level analyses of the estimated DCM parameters of single subject, we want to know the difference of mean connection strength across subjects between the simulation and perception tasks. Our experimental question was: do subjects have different driving input locations or stronger modulatory connectivity between two regions in inference task compared to perception task? And our analysis aim of connectivity parameter estimation was to test quantitative hypotheses about model parameters rather than only qualitative model structure selection.

To test hypotheses about changes in connectivity at the group level, we used hierarchical Bayesian model averaging (BMA) and comparing (BMC), which weighted the average of the connectivity parameters by the evidence of each model. To make BMA more computational efficient, we instead used Bayesian model reduction (BMR) method, which only estimate a full model (figure 4) and use the posterior estimates of this full model to derive the estimates of the reduced models, in which one or more parameters are removed. All the nested models together with the full model formed the model space.

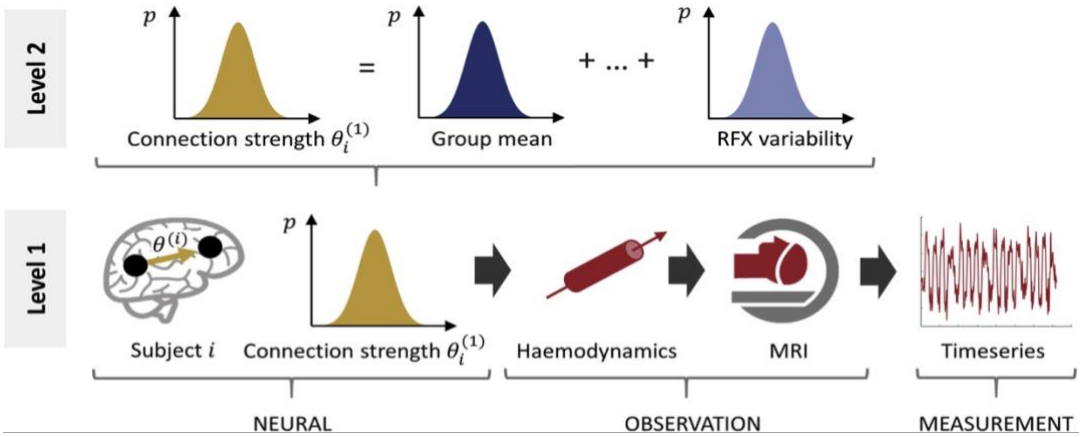

Figure 5: The two-level Parameter Empirical Bayes (PEB) model used in our analysis (8). At the first level (bottom of the figure), a forward model (DCM) describes how neural activity causes the fMRI timeseries of each subject. The parameters from the neural part of the model are taken to the group level (upper part of the figure), where they are modelled as a linear combination of a group mean and random effects (RFX) variability.

Specifically, we used the parametric empirical Bayesian (PEB) approach to estimate the connectivity parameters and their posterior probabilities on group level. In short, the PEB scheme uses BMR to invert a hierarchical Bayesian model of between subject effects on within-subject parameters, with a fancy GLM of between-subject effects (8). PEB can automatically search over all the nested models. After the full model is estimated for each subject, the full PEB model is compared against nested PEB models to test hypotheses. Parameters which don't contribute to the free energy are switched off. Finally, the average parameters over reduced DCMs weighted by their evidence are calculated to obtain a set of BMAs, representing the strength of each connection and the effects of experimental manipulations.

3. Results

3.1. Activated brain areas during inference and perception

We applied GLM analysis to both physical inference and perception tasks to identify the brain areas that have significant activations. The group-level GLM analysis of the simulation task revealed that the superior parietal lobule (SPL) and supramarginal gyrus (SMG) were largely activated during physical inference (figure 6, top row). Additionally, the perception was associated with a large increase in activities in the early visual areas (figure 6, bottom row), which is because the participants received direct visual inputs of the falling ball during the localizer task. The complete tables of the activated brain regions in both tasks can be found in the Appendix.

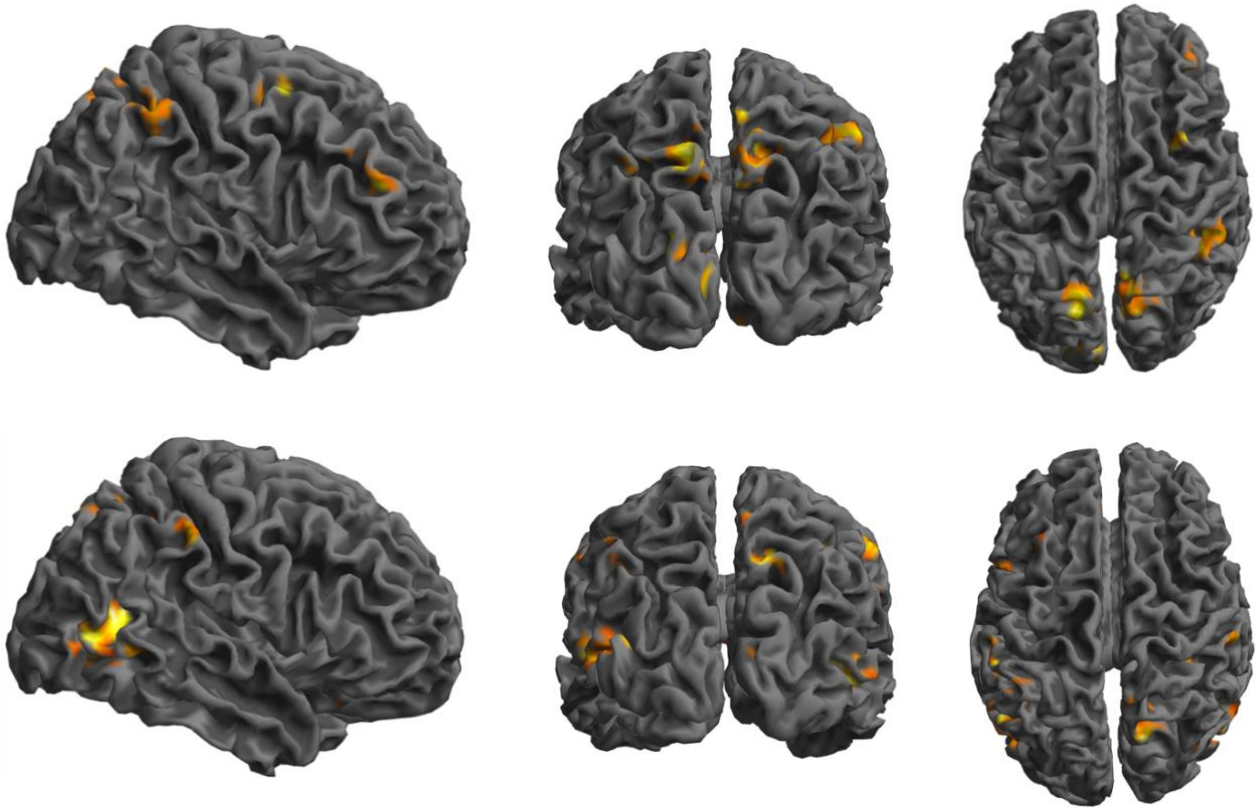

Figure 6: Brain areas that have significant activations on the group level (p<0.001 uncorrected). The upper row of the figure shows the contrast image (t-test) of GLM group level analysis of the simulation task (Inference > control). The bottom row of the figure shows the contrast image (t-test) of the perception task (perception > 0).

Furthermore, based on the conjunction analysis between the contrast image of simulation and the positive effect of perception (figure 7), we defined SPL and SMG as ROIs. The early visual cortex (V1/V2) was also selected as ROI based on its' main effect of perception. We focused our ROIs on the right hemisphere because previous study has shown that the imagery function is more associated with the right hemisphere.

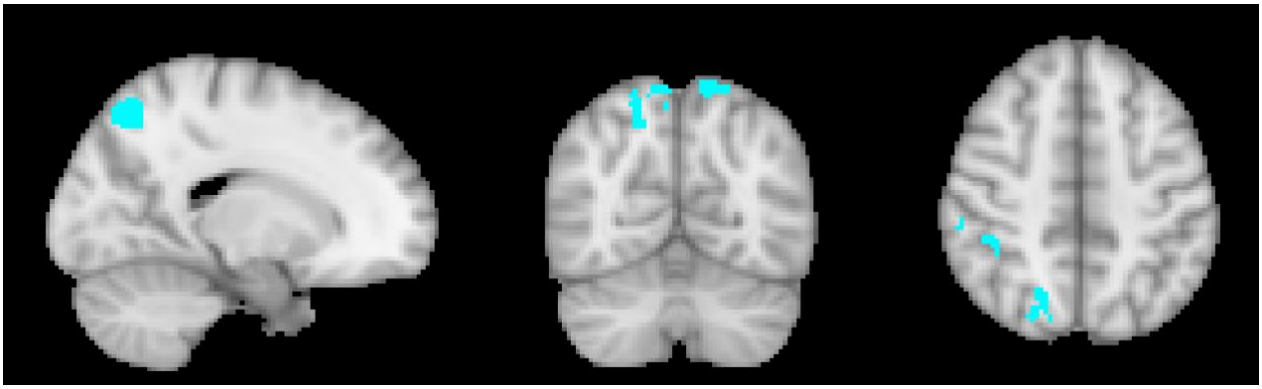

Figure 7: The conjunction analysis between the simulation and perception task selected SPL and SMG as our ROIs.

3.2. Driving input and top-down modulation during inference

We selected the fixed connectivity (A-matrix), modulatory input (B-matrix), and driving input (C-matrix) parameters respectively as the interested fields of the DCM to estimate at the group level (PEB) model. The network (figure 8) containing all the estimated parameters of effective connectivity and their posterior probabilities was concluded from the BMR results, where any effects that didn't contribute to the model evidence were pruned.

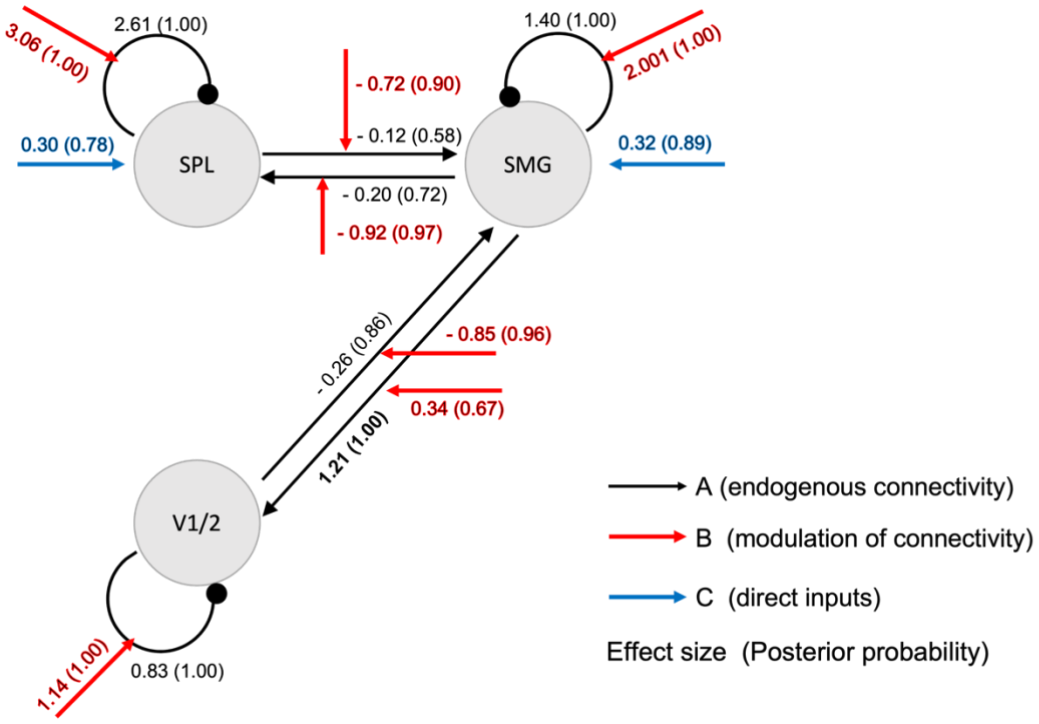

Figure 8: Network of estimated effect parameters and posterior probabilities of the fixed connectivity (A matrix, black), modulatory inputs (B matrix, red), and driving inputs (C matrix, blue) during physical inference task.

The results of PEB estimation of physical Inference task showed significant top-down excitatory modulatory inputs from SMG to Visual cortex (effect size is 0.34, posterior probability is 0.67), also with a significant increased bottom-up inhibitory modulation from Visual region to SMG (effect size is 0.85, posterior probability is 0.96). Comparing to the perception task, the physical inference task showed greater self-inhibition on the three brain regions, and greater driving inputs to higher functional brain region (SMG).

3.3. Decreased self-inhibition on visual cortex during perception

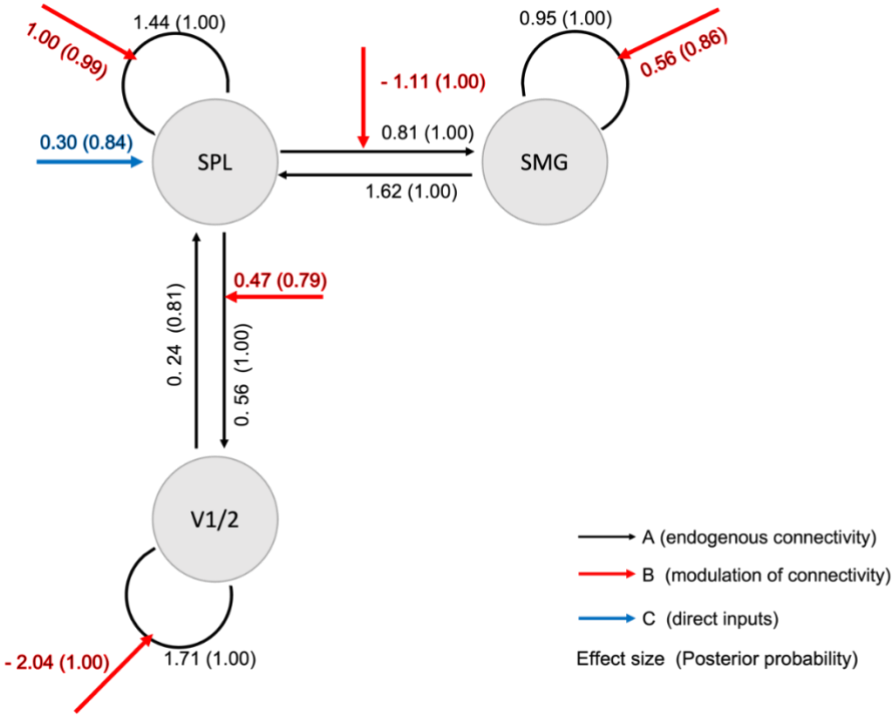

Figure 9: Network of estimated effect parameters and posterior probabilities of the fixed connectivity (A matrix, black), modulatory inputs (B matrix, red), and driving inputs (C matrix, blue) during perception task.

Additionally, the eatimated PEB parameters during the perception task (figure 9) showed decreased self-inhibition on early visual cortex (effect size is 2.04, posterior probability is 1.00). This strong disinhibition in the early visual areas revealed that visual cortex responded actively to the visual inputs of the falling ball during the perception task. The higher functional brain regions were self-inhibited and not highly involved in this visual perception task.

3.4. Comparison of connectivity strength during physical inference and perception

We also applied the BMA scheme with classical inference method such as t-tests to evaluate the difference of parameters in the estimated single-subject full models between the simulation and perception tasks.

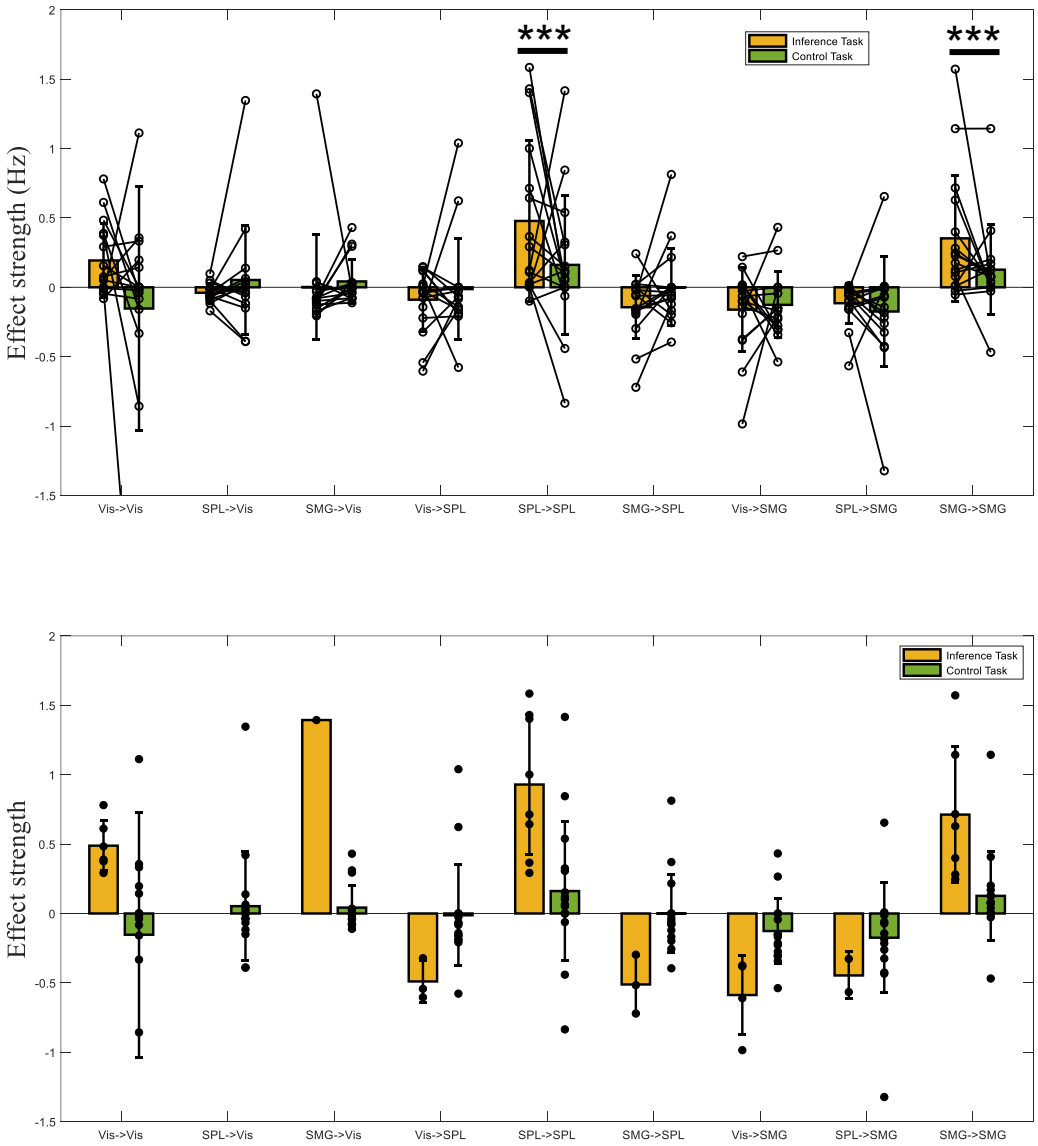

Figure 10: The upper part of the figure shows the paired t-tests between the simulation and perception tasks of each subject's estimated modulatory inputs of the full model. Comparisons that have statistically highly significant difference ($p<0.001$) are indicated with ***. The bottom panel of the figure shows the histogram of each subject's estimated parameters of the B-matrix in the full model with posterior probabilities over 0.7.

The classical paired t-test comparisons of the estimated single-subject full models (figure 10, top panel) failed to provide enough useful information on the difference between the two tasks, because it ignored the uncertainty at the between-subject level and assumed every subject contributed equally well to the group estimation of parameters. To remedy this issue, we set a threshold 0.7 of posterior probabilities to remove the low-quality estimation from the group parameters comparison. The subsequent results (figure 10, bottom panel) of classical inference revealed similar conclusions as PEB estimation, that supported PEB is a more reliable and robust method of group-level parameters inference.

4. Discussion

Our hypothesis is that physical inference is associated with higher functional brain areas and may involve visual imagery, whereas the perception task involves more of the visual cortex only. And the fMRI data modelling results largely support our hypothesis. The significant driving inputs to SMG and SPL and top-down modulation during simulation task suggested that during physical inference, the higher functional brain regions are activated first and transmit the prior physical knowledges down to the visual areas allowing the subjects to virtually “see” the trajectory of the falling ball. In contrast, the direct visualization of the falling ball only activated the local neural activities in the visual cortex.

During DCM and the following PEB analysis, we found that the modelling results are sensitive to the model specification and F-test adjustion, so in the following analysis we can apply more advanced DCM methods to help establish more robust conclusions. To investigate the neural mechanism of physical inference in human, we implemented the fMRI experiments with a single body motion inference and the parallel comparison experiment. In the future we can design other forms of object motion inference experiments to further build the neural dynamic networks of physical inference mechanism.

5. References

1. Battaglia, Peter W., Jessica B. Hamrick, and Joshua B. Tenenbaum. "Simulation as an engine of physical scene understanding." *Proceedings of the National Academy of Sciences* 110.45 (2013): 18327-18332.

2. Albers, Anke Marit, et al. "Shared representations for working memory and mental imagery in early visual cortex." *Current Biology* 23.15 (2013): 1427-1431.

3. Fischer, Jason, et al. "Functional neuroanatomy of intuitive physical inference." *Proceedings of the national academy of sciences* 113.34 (2016): E5072-E5081.

4. Eickhoff, Simon B., et al. "A new SPM toolbox for combining probabilistic cytoarchitectonic maps and functional imaging data." *Neuroimage* 25.4 (2005): 1325-1335.

5. Dijkstra, Nadine, et al. "Distinct top-down and bottom-up brain connectivity during visual perception and imagery." *Scientific reports* 7.1 (2017): 1-9.

6. Stephan, Klaas E., et al. "Translational perspectives for computational neuroimaging." *Neuron* 87.4 (2015): 716-732.

7. Zeidman, Peter, et al. "A guide to group effective connectivity analysis, part 1: First level analysis with DCM for fMRI." *Neuroimage* 200 (2019): 174-190.

8. Zeidman, Peter, et al. "A guide to group effective connectivity analysis, part 2: Second level analysis with PEB." *Neuroimage* 200 (2019): 12-25.

A. Appendix

Cluster	JuBrain V3.0 Atlas	Harvard-Oxford Atlas	Size (voxels)	T	Peak location		
1	Occipital lobe L Area hOc1 [V1] 19.9%	Supracalcarine Cortex 5.9%	362	7.39	-30	-64	-2
2	Frontal lobe R Area 6mr / preSMA 1.3%	Paracingulate Gyrus 70.0% Superior Frontal Gyrus 5.0%	350	6.71	2	18	46
3	Parietal lobe R (SMG) Area hIP1 (IPS) 45.1% Area hIP2 (IPS) 38.1% Area PGa (IPL) 5.7% Area hIP3 (IPS) 4.9%	Angular Gyrus 32.0% Supramarginal Gyrus, posterior division 26.0%	296	5.39	44	-46	48
4	Parietal lobe R Area 7A (SPL) 27.8% Area 7P (SPL) 22.3%	Lateral Occipital Cortex, superior division 39.0% Precuneous Cortex 12.0%	256	6.31	12	-66	56
5	Parietal lobe L Area 7A (SPL) 26.4% Area hIP8 (IPS) 21.9% Area 7P (SPL) 20.8%	Lateral Occipital Cortex, superior division 50.0% Precuneous Cortex 12.0%	248	6.23	-12	-72	54
6	Frontal lobe R Area 6d3 9.5%	Middle Frontal Gyrus 31.0% Precentral Gyrus 13.0%	243	6.39	32	0	54
7	Occipital lobe L Area hOc4d [V3A] 49.8% Area hOc3d [V3d] 44.2% Area hOc2 [V2] 6.0%	Occipital Pole 44.0% Lateral Occipital Cortex, superior division 17.0%	210	6.72	-20	-92	22
8	R	Frontal Pole 67.0% Middle Frontal Gyrus 3.0%	87	5.89	38	42	24
9	Occipital lobe R Area hOc1 [V1] 20.7%		79	5.53	22	-78	2
10	Occipital lobe R Area hOc3v [V3v] 38.5% Area hOc2 [V2] 5.0%	Cerebellum Right VI 90.5% Cerebellum Right Crus I 4.8%	62	5.37	22	-70	-20

Table 1: This table summarizes the clusters that are identified by the GLM group-level t-test (Simulation > Control) analysis, which only includes the clusters larger than 50 voxels.

Cluster	JuBrain V3.0 Atlas	Harvard-Oxford Atlas	Size (voxels)	T	Peak location		
1	Occipital lobe L Area hOc5 [V5/MT] 9.1% Area hOc4la 8.8%	Lateral Occipital Cortex, inferior division 26.0% Middle Temporal Gyrus, temporooccipital part 22.0%	403	8.12	-52	-62	12
2	Area hOc5 [V5/MT] 26.1% R Area hOc4la 11.2%	Lateral Occipital Cortex, inferior division 33.0% Lateral Occipital Cortex, superior division 15.0%	389	9.89	42	-62	14
3	Parietal lobe R Area 7P (SPL) 66.0% Area 7A (SPL) 11.9%	Lateral Occipital Cortex, superior division 55.0% Precuneous Cortex 10.0%	120	6.18	14	-76	50
4	Area hIP3 (IPS) 36.5% R Area hIP1 (IPS) 33.6% Area hIP2 (IPS) 20.3%	Supramarginal Gyrus, posterior division 31.0% Superior Parietal Lobule 6.0%	77	5.1	38	-38	38
5	Area PF (IPL) 41.1% R Area PFt (IPL) 22.6%	Supramarginal Gyrus, anterior division 84.0% Postcentral Gyrus 2.0%	59	5.45	60	-28	46
6	Frontal lobe L Area 44 64.8%	Inferior Frontal Gyrus, pars opercularis 35.0% Precentral Gyrus 32.0%	57	5	-50	8	22
7	Area PFt (IPL) 65.9% L Area PF (IPL) 17.5% Area PFop (IPL) 1.1%	Supramarginal Gyrus, anterior division 50.0% Postcentral Gyrus 26.0%	45	5.64	-58	-28	40

Table 2: This table summarizes the clusters that are identified by the GLM group-level t-test (Positive effects of localizer Fall) analysis, which only includes the clusters larger than 30 voxels.